

## Article

# Medium-Temperature Phosphate Glass Composite Material as a Matrix for the Immobilization of High-Level Waste Containing Volatile Radionuclides

Anna V. Frolova , Sergey E. Vinokurov \*, Irina N. Gromyak and Sergey S. Danilov

Vernadsky Institute of Geochemistry and Analytical Chemistry of Russian Academy of Sciences, 19 Kosygin St., 119991 Moscow, Russia

\* Correspondence: vinokurov.geokhi@gmail.com

**Abstract:** The search for matrices and technological solutions for the reliable immobilization of volatile radionuclides and high-level waste (HLW) components is an actual radiochemical problem. Methods of obtaining of sodium alumino-iron phosphate (NAFP) and iron phosphate (FP) glass composite materials synthesized at temperatures of 450–750 °C, their structure and hydrolytic stability were investigated in this paper. The structure of the samples was studied by XRD and SEM-EDS. It was shown that, in the case of FP materials, the phase composition varies depending on the synthesis temperature, while NAFP materials have a complex multiphase composition at all crystallization temperatures. It has been established that the samples of the obtained glass composite materials have a high hydrolytic stability. At the same time, FP material obtained at 650 °C are the most stable, which makes this medium-temperature method of synthesis promising for the immobilization of volatile HLW components.

**Keywords:** phosphate glass; sodium alumino-iron phosphate glass; phosphate glass composite materials; ceramics; radioactive waste; high-level waste; immobilization; leaching; structure



**Citation:** Frolova, A.V.; Vinokurov, S.E.; Gromyak, I.N.; Danilov, S.S. Medium-Temperature Phosphate Glass Composite Material as a Matrix for the Immobilization of High-Level Waste Containing Volatile Radionuclides. *Energies* **2022**, *15*, 7506. <https://doi.org/10.3390/en15207506>

Academic Editor: Abdul-Ghani Olabi

Received: 15 September 2022

Accepted: 9 October 2022

Published: 12 October 2022

**Publisher's Note:** MDPI stays neutral with regard to jurisdictional claims in published maps and institutional affiliations.



**Copyright:** © 2022 by the authors. Licensee MDPI, Basel, Switzerland. This article is an open access article distributed under the terms and conditions of the Creative Commons Attribution (CC BY) license (<https://creativecommons.org/licenses/by/4.0/>).

## 1. Introduction

One of the most important tasks of the nuclear power industry is to ensure the radiation-safe management of radioactive waste (RW). Among the already accumulated waste, high-level waste (HLW) is especially dangerous. First of all, in some countries HLW is spent nuclear fuel (SNF), which includes fission products, actinides, and elements of fuel assemblies. After 5 years of storage with SNF burnup 40 (GW day/t HM), significant elements in SNF will be kg/t:  $^{235,236}\text{U}$ —17, REE—16, Pu—9.9, Zr—5.2, Cs—5.1, Mo—4.2, Sr—1.4, and Tc—1.1 [1]. At the same time, in some other countries, in particular in Russia and France, it is planned to further process SNF in order to extract actinides and fractionate waste [2,3]; therefore, different compositions of HLW are possible. The multi-barrier concept was proposed for the reliable isolation of RW, according to which the barriers are metal and/or concrete canisters/containers containing RW, included in a safe matrix, essentially the first barrier, clay (buffer materials) and naturally occurring wall rocks (e.g., granite) [4]. Deep geological disposal in the implementation of the multi-barrier concept is the preferred solution for the final disposal of HLW [5]. In the 1950s, a vitrification process was proposed to convert waste into a safe form [6]. Borosilicate and aluminophosphate glasses are considered the most promising glass matrices [4]. Vitrification, however, being an industrial method for HLW removal, has a number of disadvantages and is unsuitable for some types of waste. It is known that the glass structure changes at high temperature, pressure, and the ingress of water, as a result of which radionuclides can be washed out by water. In the 1970s, the popular Synroc ceramic was proposed in Australia. This is a titanium ceramic based on the minerals zirconolite  $\text{CaZrTi}_2\text{O}_7$ , hollandite  $\text{Ba}_{1,2}(\text{Al,Ti})_8\text{O}_{16}$ , perovskite  $\text{CaTiO}_3$  and titanium oxides  $\text{Ti}_n\text{O}_{2n-1}$ , mainly rutile  $\text{TiO}_2$  [7–9].

The idea of using ceramics came from the stability of naturally occurring minerals containing natural radionuclides. Their stability of the order of hundred thousand years is not in doubt [10]. Among the many potential advantages of ceramics are the low rate of radionuclide leaching, long life and resistance to radiation exposure, high loading of waste components, thermal and mechanical stability and ease of synthesis [11]. Glass ceramics and glass composite materials [12–15], which can be obtained by different methods, including the slow cooling of a glass melt [16], have been extensively studied as promising matrices for radionuclide incorporation. Other methods for the synthesis of glass composite materials are cold and hot uniaxial pressing, hot isostatic pressing, liquid-phase sintering, and the sintering of viscous composites [17].

It should be noted that glasses and ceramics have a high synthesis temperature. Thus, the synthesis temperature of borosilicate glass is approximately 1150 °C [18], phosphate—900–1050 °C [19], and for some types of single-phase ceramics, the synthesis temperature can reach 1700–1800 °C [20]. Such high synthesis temperatures can prevent the immobilization of volatile radionuclides. According to [21], during the synthesis of borosilicate glass at 1150–1250 °C,  $^{99}\text{Tc}$  can volatilize up to 90% from the composition of the solidified waste. A similar problem is also relevant for wastes containing cesium isotopes and/or chlorides. Vitrification has been recognized as an inefficient way to immobilize chloride waste generated from the pyrochemical processing of spent nuclear fuel (SNF) [22]. It should be noted that, over time, such waste is likely to accumulate in large quantities. Thus, in Russia, such waste will be generated from the processing of the mixed uranium–plutonium SNF (MNUP SNF) of the BREST-OD-300 reactor plant with lead coolant [23]. In the US, waste from the EBR-II research reactor is subject to pyrochemical processing [24]. It was shown in [25,26] that matrices of the “zeolite/sodalite in glass” type can be promising for such wastes.

Attempts to optimize the process by making it less high-temperature have been made. For example, in [27], chlorapatite and borosilicate glass were sintered to obtain a matrix for chloride-waste immobilization. It is known that glass composite materials can be produced using lower temperatures than glass melting [28]. The process of sintering crushed glass seems interesting [29,30]. In this approach, the synthesis of the matrix is possible at average temperatures of 550–750 °C, and an increase in the stages of synthesis is not associated with the possible spread of radioactivity.

Previously, we considered sodium-aluminum-iron-phosphate glass (NAFP), which has a lower synthesis temperature compared to aluminophosphate glass [31], as well as a magnesium–potassium–phosphate (MPP) compound produced at room temperature [32], as promising matrices for the immobilization of volatile wastes. Both proposed matrices had their own advantages and disadvantages in spent electrolyte immobilization [33]. The glass demonstrated high radiation resistance upon irradiation up to a dose of  $10^9$  Gy and resistance to leaching but had weakly included chlorine in its composition. Some authors note ([34]) that the removal of inactive chlorine during synthesis is not a problem, but this can complicate the technology. The incorporation of rhenium as a technetium simulant in NAFP glass was about 70% [31]. The easy-to-synthesize low-temperature MPP matrix included a quantitatively larger amount of the spent electrolyte simulant but tended to decrease in strength under thermal loads.

The aim of this study was to investigate the possibility of obtaining a stable iron phosphate glass composite material at medium temperatures to immobilize volatile radionuclides and RW types unsuitable for incorporation in high-temperature glass matrices.

## 2. Materials and Methods

### 2.1. Chemicals and Procedures

Known stable compositions of iron phosphate glass were chosen as promising for sintering glass composite materials at medium temperatures. Thus, a simple two-component glass matrix of composition mol%,  $40\text{Fe}_2\text{O}_3\text{-}60\text{P}_2\text{O}_5$  (FP glass), is recognized as hydrolytically and chemically stable and has a high waste-loading capacity [35]. Upon slow cooling (annealing), this glass is prone to the formation of iron orthophosphates or pyrophosphates,

depending on the temperature and holding conditions [36]. At the same time, crystallized forms retain high hydrolytic stability.

NAFP matrix composition mol%:  $40\text{Na}_2\text{O}-10\text{Al}_2\text{O}_3-10\text{Fe}_2\text{O}_3-40\text{P}_2\text{O}_5$  was also chosen as promising for medium-temperature synthesis. This glass has high crystallization and hydrolytic stability [37,38]. The composition is in the region between ortho- and pyrophosphate; upon prolonged annealing, it forms predominantly pyrophosphate structure. The conditions for the synthesis of the studied compounds are presented below.

The original blank samples of FP and NAFP glass containing no waste were synthesized by melting up to  $1100\text{ }^\circ\text{C}$  in quartz crucibles with the isothermal holding of the resulting melts for 1 h and then pouring them onto a metal sheet for glass quenching. The calculated elemental composition of the samples (wt%) is given in Table 1. A batch of glass was prepared from a mixture of dry components  $(\text{NH}_4)_2\text{HPO}_4$  (GOST 3772-74),  $\text{Na}_2\text{CO}_3$  (GOST 4530-76)  $\text{Al}_2\text{O}_3$  (TU 6-09-426-75) and  $\text{Fe}_2\text{O}_3$  (TU 6-09-5346-87) (Len-reactiv, Saint Petersburg, Russia). It is possible to include a certain amount of  $\text{SiO}_2$  from the crucible into melts during synthesis in quartz crucibles. In order to prevent the excess boiling and consequent spillage, the batches were previously calcined at  $450\text{ }^\circ\text{C}$  for 4 h in a muffle furnace SNOL 30/1300 (AB UMEGA GROUP, Utena, Lithuania) to remove water and ammonia in ammonium dihydrogen phosphate initially.

**Table 1.** Estimated elemental composition of FP and NAFP glass samples, wt%.

Element	FP	NAFP
P	24.9	23.0
Fe	30.0	10.4
Na	-	17.1
Al	-	5.0
O	45.1	44.6

After that, the obtained glasses were manually ground in an agate mortar, and a fraction of particles with a size of less than 0.07 mm was sifted using a vibrating sieve analyzer Hsiangtai LS-300 (Hsiangtai Machinery Industry, Taipei, Taiwan) at a frequency of 3000 rpm. In the future, after this stage, it is supposed to transfer the obtained glass powder to the hot zone for the introduction of calcined RW and mixing with glass powder. Tablets with a diameter of 10 mm from crushed powders were pressed under a pressure of 3–4 MPa using a PGR-10 hydraulic press (LabTools, Saint Petersburg, Russia). It is assumed that pressing can prevent the undesirable remelting of crushed glass and promote their sintering into a glass composite material. The tablets obtained were sintered at 450, 550, 650 and  $750\text{ }^\circ\text{C}$  for 6 h in a muffle furnace SNOL 30/1300 on a stainless steel substrate. The lowest temperature of  $450\text{ }^\circ\text{C}$  was chosen because of the crystallization processes that begin at this temperature in phosphate glass [39,40], which was supposed to be enhanced by preliminary grinding.

## 2.2. Methods

The phase composition of the obtained samples was identified by the X-ray diffraction (XRD) method using a diffractometer Ultima-IV (Rigaku, Tokyo, Japan). The XRD data were interpreted using the Smartlab Studio II program package (Rigaku, Tokyo, Japan) with the PDF-2 powder database. The microstructure of the FP was investigated by the scanning electron microscopy (SEM) using a microscope Mira3 (Tescan, Brno, Czech Republic), and the electron probe microanalysis of the samples was performed by energy-dispersive X-ray spectroscopy (EDS) using an analyzer X-Max (Oxford Inst., High Wycombe, UK).

The hydrolytic stability of the samples obtained was determined in accordance with the static method PCT [41]. For this, fractions of crushed sintered tablets with a particle size of 0.01–0.02 mm and a mass of about 1 g were used. The powders were washed with bidistilled water and alcohol before testing to avoid the possibility of the ingress of the dust fraction of the sample. The powders were placed in a plastic container, poured into

10 mL of bidistilled water, and thermostated at  $90 \pm 2$  °C in a laboratory oven SCHS-80-01 (SKTB SPU, Smolensk, Russia) for 7 days. The obtained leachates were decanted and centrifuged for 5 min at 8000 rpm in a CLN-16 centrifuge (Changsha Xiangzhi Centrifuge Instrument, Changsha, China). The content of the components in the solution after leaching was determined by ICP–AES (iCAP-6500 Duo, Thermo Scientific, Waltham, MA, USA).

The normalized leaching rate LR, [g/(cm<sup>2</sup>·day)], of the components was calculated by Equation:

$$LR = \frac{c \cdot V}{S \cdot f \cdot t},$$

where c—element concentration in solution after leaching, g/L; V—the volume of leaching agent, L; S—the sample surface (the geometrical parameters of the tablet samples were measured with a caliper), cm<sup>2</sup>; f—mass fraction of the element in matrix, g/g; t—duration of the leaching period, days.

### 3. Results and Discussion

#### 3.1. Geometric Parameters and Density of Glass Composite Material Tablets

The appearance of the obtained samples of FP and NAFP matrices is shown in Figure 1. It can be seen that the samples sintered at different temperatures differ in color, which is probably due to the different composition of the resulting crystalline phases. Samples sintered at 450 °C turned out to be brittle. Samples sintered at 550–750 °C formed dense tablets.

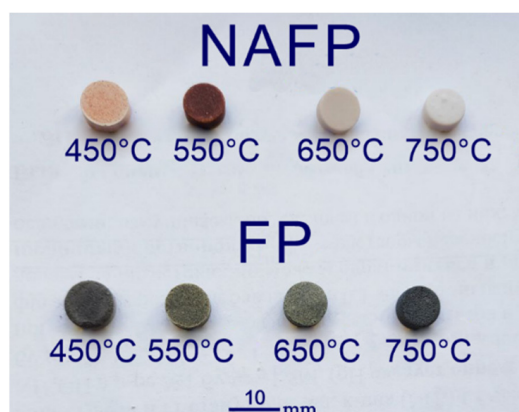


**Figure 1.** Appearance of the obtained samples of FP and NAFP matrices.

The geometric dimensions of the samples and the density of NAFP and FP glass before sintering and glass composite material after sintering are presented in Table 2, the measurement error was  $\pm 0.05$  mm. An increase in the density of sintered matrices is a desirable parameter, since strength characteristics are an important criterion for compounds during RW immobilization. The trend towards an increase in the density of the resulting NAFP and FP matrices tablets can be observed for all samples at a sintering temperature above 550 °C.

**Table 2.** Geometrical parameters of samples NAFP and FP matrices at different synthesis temperatures, where d—diameter of tablet (mm), h—height of tablet (mm),  $\rho$ —density (g/cm<sup>3</sup>).

Sample	Parameters	before Synthesis	450 °C	550 °C	650 °C	750 °C
FP	d	10.10	10.10	9.45	9.38	9.20
	h	3.60	3.60	3.50	3.45	3.40
	$\rho$	2.12	2.12	2.44	2.52	2.52
NAFP	d	10.10	10.10	10.10	9.15	9.15
	h	3.80	3.80	3.80	3.55	3.50
	$\rho$	1.97	1.97	1.97	2.57	2.62

### 3.2. Characterization of the Synthesized Compounds by XRD and SEM/EDS

The obtained XRD patterns of the FP samples are shown in Figure 2. The sample synthesized at 450 °C (Figure 2a) was found to be amorphous and glasslike. Obviously, the temperature turned out to be low for the start of crystallization processes in iron phosphate glass, despite the preliminary grinding. It is shown that samples of FP matrices synthesized at 550 and 650 °C (Figure 2b,c, respectively) are partially crystallized and are represented by both an amorphous phase and phosphate phases. In the sample synthesized at 550 °C, the only crystalline phase is iron orthophosphate. In the sample synthesized at 650 °C, the main phases are the crystalline phases of iron orthophosphate and iron pyrophosphate. The sample of the FP matrix synthesized at 750 °C (Figure 2d) is completely represented by the pyrophosphate structure.

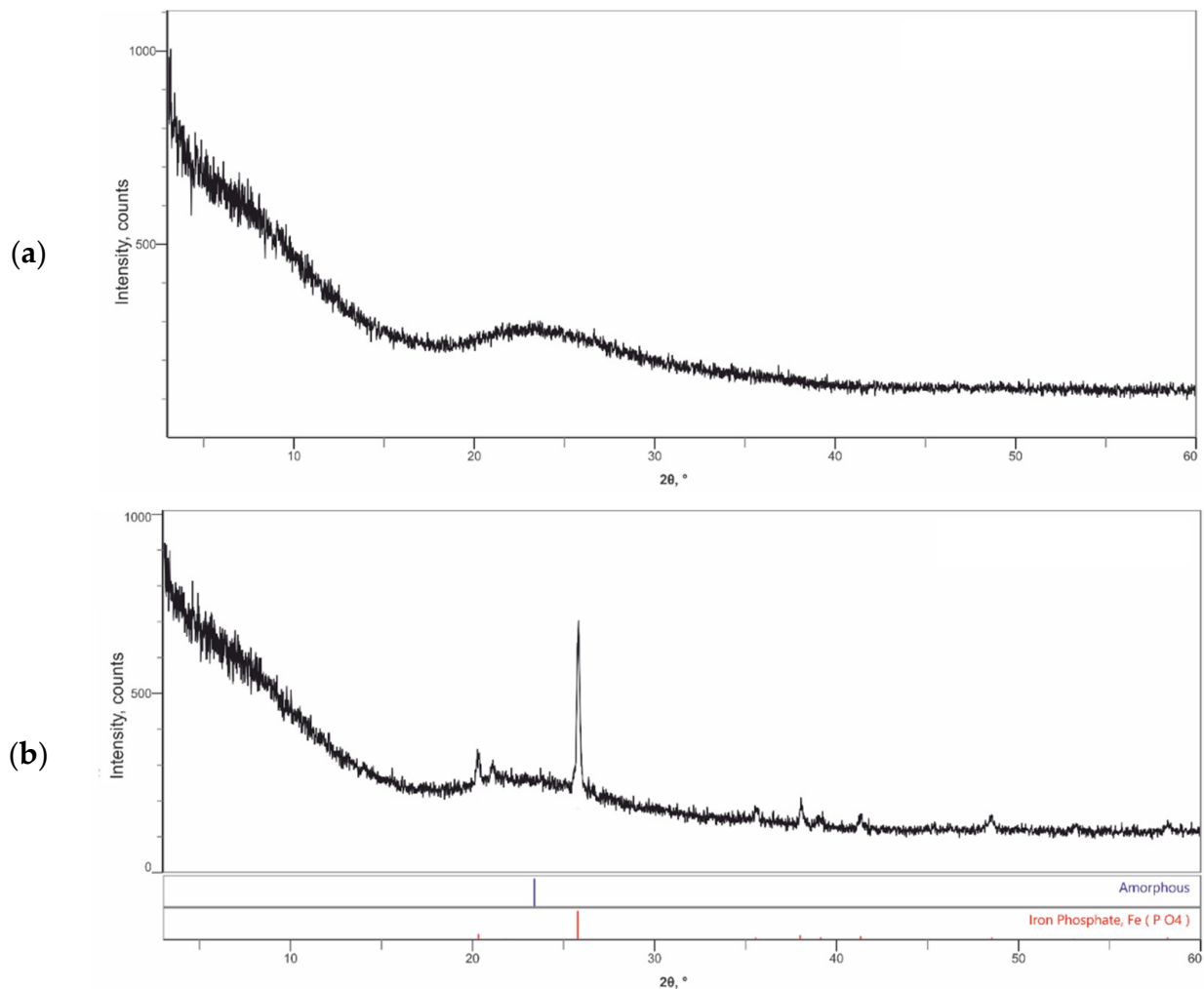
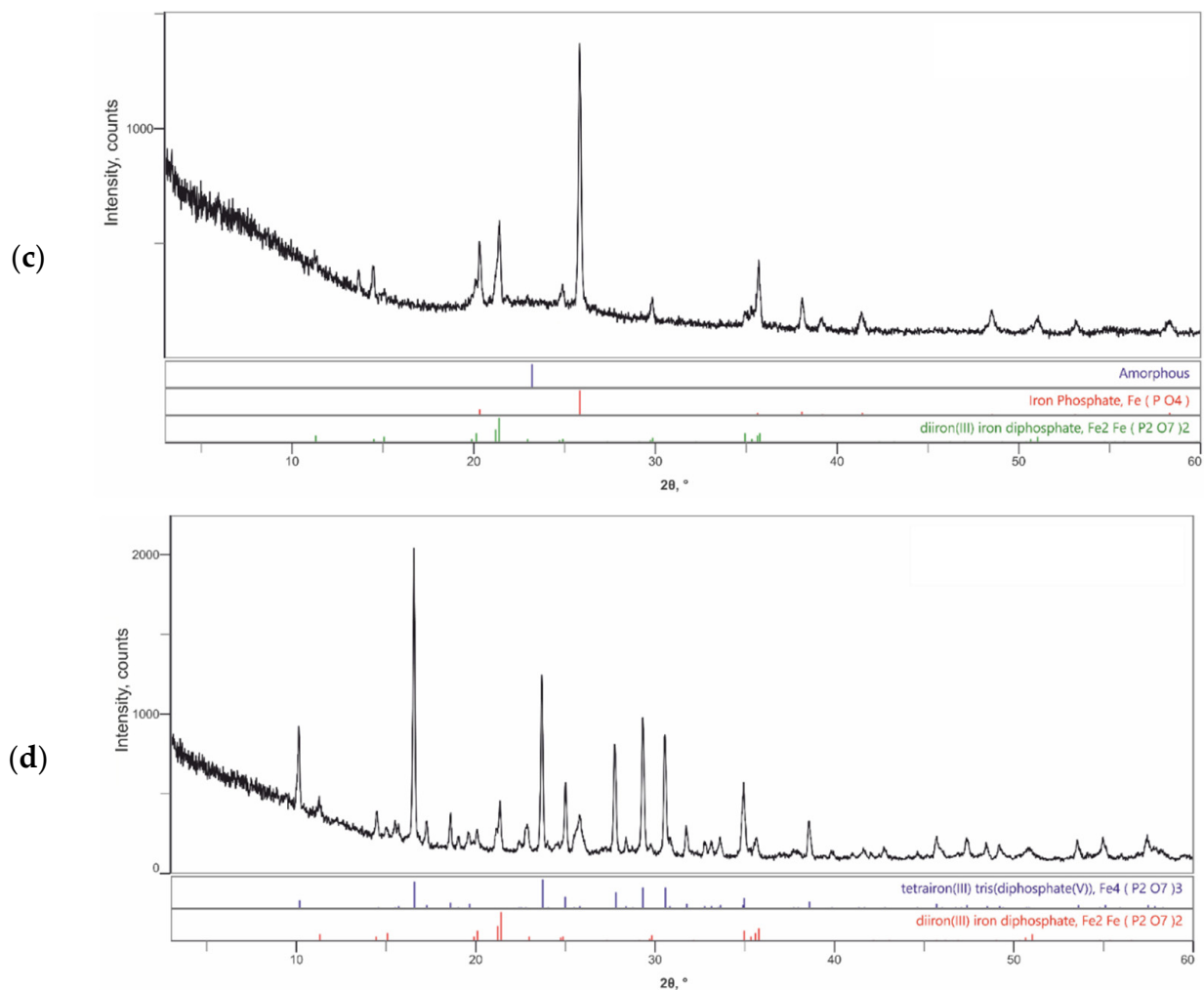
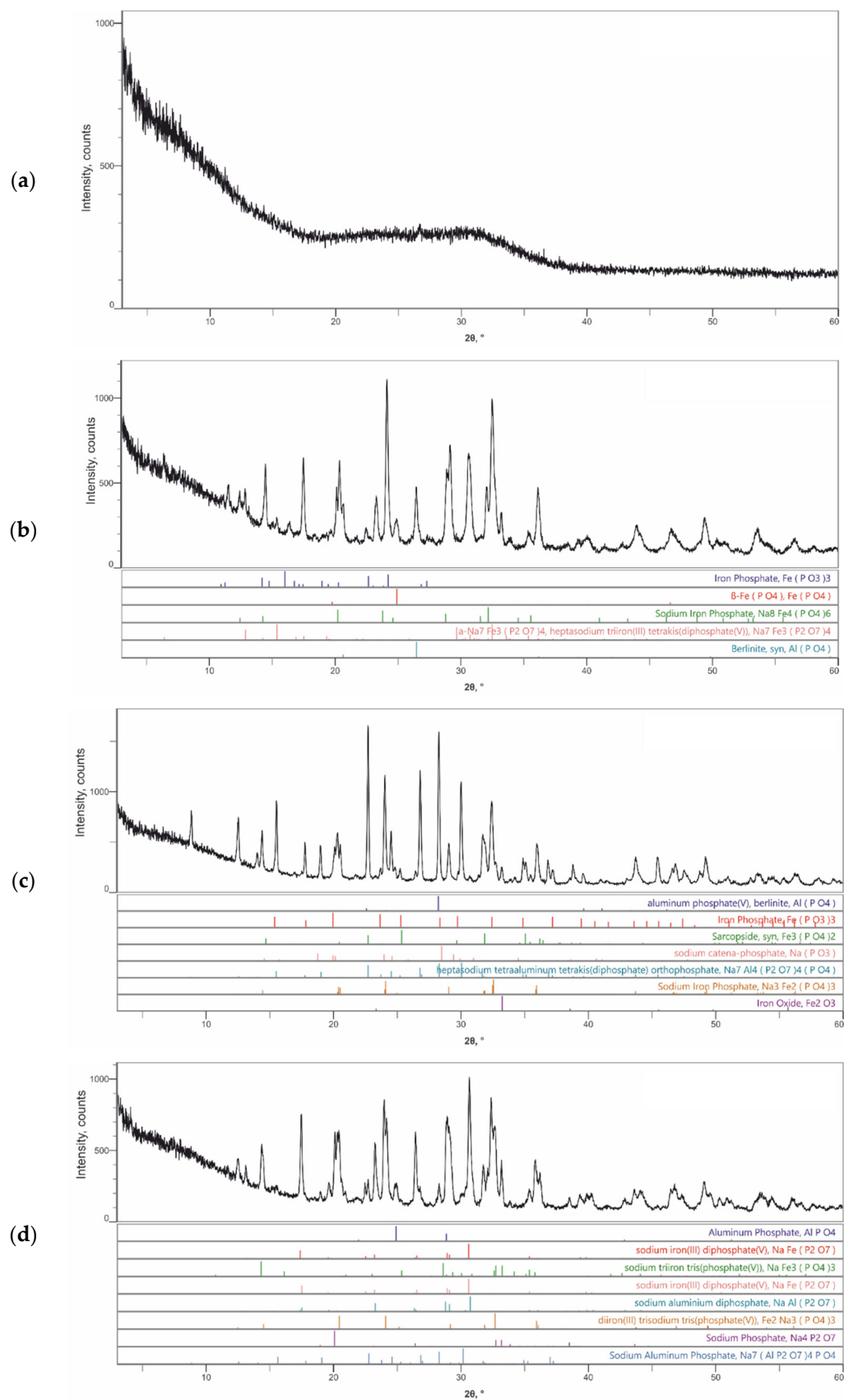


Figure 2. Cont.



**Figure 2.** X-ray diffraction patterns of FP matrix samples synthesized at 450 (a), 550 (b), 650 (c) and 750 °C (d).

The obtained XRD patterns of the NAFP matrix samples are shown in Figure 3. It is shown that the sample synthesized at 450 °C (Figure 3a) is completely amorphous, as in the case of the FP sample. Samples of NAFP matrices synthesized at 550–750 °C (Figure 3b–d) are completely crystallized; do not have an amorphous phase; and consist of a complex composition of meta-, ortho-, and pyrophosphates. The sample synthesized at 550 °C (Figure 3b) was found to be formed by iron metaphosphate, iron and aluminum orthophosphates, as well as mixed sodium iron orthophosphate, and sodium iron pyrophosphate. The NAFP sample synthesized at 650 °C (Figure 3c) consists of iron and sodium metaphosphates; aluminum, iron and sodium-iron orthophosphates; and heptasodium tetraaluminium (diphosphate) orthophosphate. Iron oxide is probably an impurity phase that passed to the surface of the glass composite matrix during sintering. The synthesis of a NAFP matrix at 750 °C (Figure 3d) leads to the formation of aluminum and sodium-iron orthophosphates, sodium-iron and sodium-aluminum pyrophosphates, and heptasodium tetraaluminium (diphosphate) orthophosphate. Thus, the NAFP matrix has a more varied phase composition and does not show the prevalence of any predominant phosphate structure depending on the synthesis temperature.



**Figure 3.** X-ray diffraction patterns of NAFP matrix samples synthesized at 450 (a), 550 (b), 650 (c) and 750 °C (d).

SEM micrographs of the surface of the obtained at 550–750 °C. FP matrices are shown in Figure 4. The sample obtained at 450 °C was not analyzed due to its brittleness. The phase composition is presented in Table 3. It was shown that the distribution of elements over the sample is homogeneous, and the phase composition approximately corresponds to the calculated one (Phase #1, Table 3), except for the sample synthesized at 750 °C (Figure 4c), wherein the phase (Phase #2) contains molybdenum from the surface composition of the sample incorporated from the substrate during synthesis.

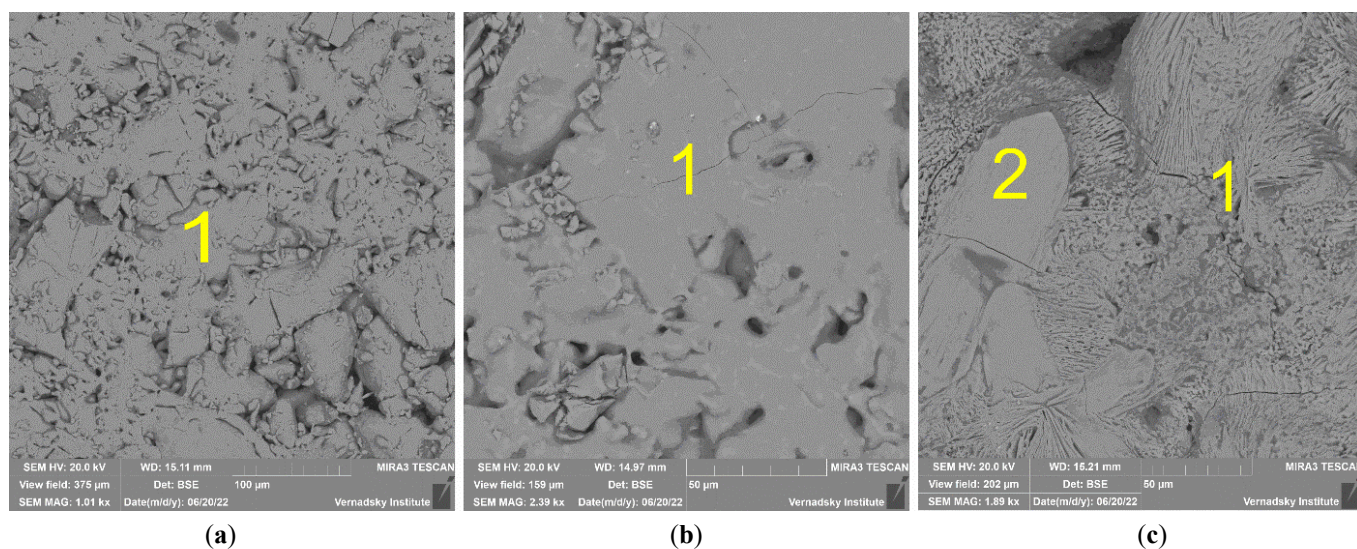


**Figure 4.** SEM micrographs of FP matrix samples synthesized at 550 (a), 650 (b) and 750 °C (c), where 1 and 2 are phosphate phases.

**Table 3.** Average data of elemental composition (wt%) of the FP matrix according to SEM/EDS data.

Element	Phase #1	Phase #2
P	24.5 ± 2.4	23.5 ± 2.3
Fe	30.7 ± 3.1	30.8 ± 3.1
O	44.8 ± 4.5	44.3 ± 4.4
Mo	-	1.5 ± 0.2

SEM micrographs of the surface of NAFF glass composite matrices obtained at 550–750 °C is shown in Figure 5. The amorphous sample synthesized at 450 °C was also too brittle for analysis. Samples synthesized at 550–750 °C are inhomogeneous and consist of at least two different visible phases. In all samples, there is a main phase (Phase #1, Table 4) with a similar composition but that differs from the calculated one by a slightly higher iron content. Due to the complex phase composition of the samples (Figure 3), it was difficult to determine the predominant phase. The darker Phase #2 and Phase #4 in the NAFF samples (Figure 5a,c), synthesized at 550 and 750 °C, respectively, are characterized by an even higher iron content (Table 4). However, the content of sodium and aluminum in them is different, which indicates the prevalence of various mixed, predominantly ferrous phosphates in each of the phases. The lighter Phase #3 (Table 4, Figure 4b) in the sample synthesized at 650 °C, on the contrary, contains slightly less iron but more aluminum and sodium. Thus, in NAFF samples, a much less homogeneous distribution of phases on the surface of the samples is observed.

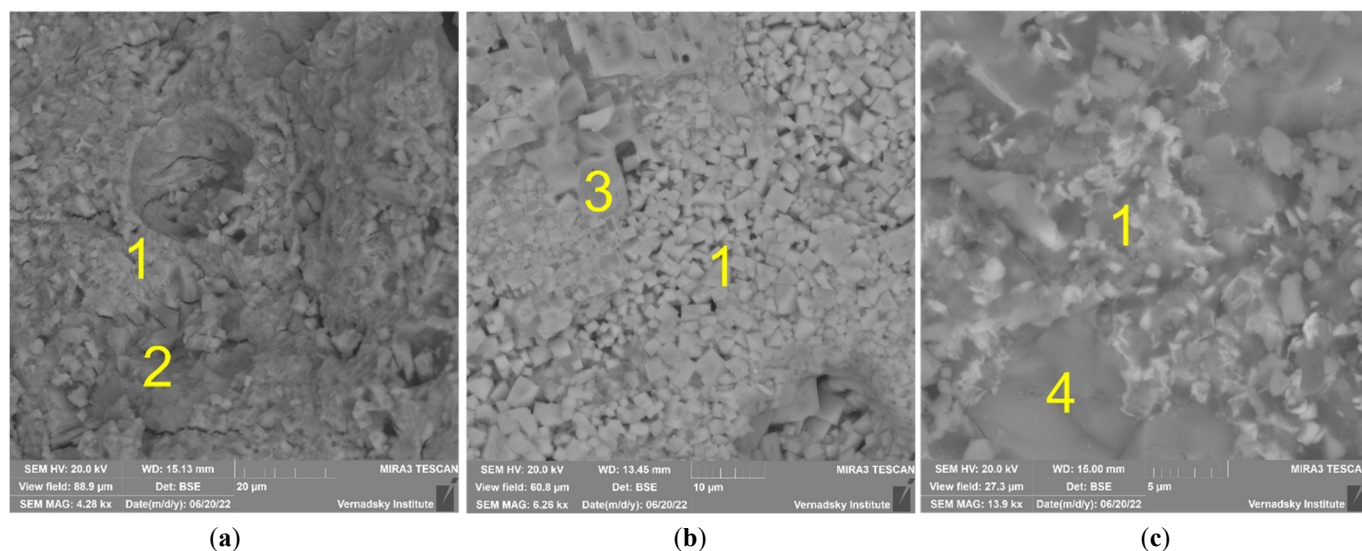


**Figure 5.** SEM image of NAFP matrix samples synthesized at 550 (a), 650 (b) and 750 °C (c), where 1, 2, 3 and 4 are phosphate phases.

**Table 4.** Average data of elemental composition (wt%) of the NAFP matrix according to SEM/EDS data.

Element	Phase #1	Phase #2	Phase #3	Phase #4
P	22.3 ± 2.2	23.8 ± 2.4	24.5 ± 2.4	20.8 ± 2.1
Fe	12.1 ± 1.2	16.3 ± 1.6	9.4 ± 0.9	20.5 ± 2.1
Na	16.0 ± 1.6	9.5 ± 0.9	14.1 ± 1.4	14.0 ± 1.4
Al	5.9 ± 0.8	5.1 ± 0.7	6.1 ± 0.8	2.2 ± 0.3
O	43.4 ± 4.3	44.4 ± 4.4	45.9 ± 4.6	42.5 ± 4.3
Si	0.3 ± 0.1	1.0 ± 0.2	-	0.24 ± 0.1

### 3.3. Hydrothermal Resistance of Glass Composite Matrices in PCT Standard Test

The data on the leaching rate of compound components are represented in Table 5. It is shown that glass composite matrix samples have high hydrolytic stability at  $90 \pm 2$  °C, while the lowest leaching rates are typical for FP matrix samples. Thus, the rate of phosphorus leaching from FP samples synthesized at 650 and 750 °C is  $5.7 \times 10^{-7}$  и  $3.9 \times 10^{-7}$  g/(cm<sup>2</sup>·day), respectively, and iron— $5.7 \times 10^{-7}$  и  $7.9 \times 10^{-7}$  g/(cm<sup>2</sup>·day), respectively.

**Table 5.** The normalized leaching rate of NAFP and FP matrices components according to the PCT standard test.

Sample	Temperature Synthesis	P	Fe	Na	Al
FP	450	$1.0 \times 10^{-6}$	$1.1 \times 10^{-7}$	-	-
	550	$6.5 \times 10^{-7}$	$1.1 \times 10^{-7}$	-	-
	650	$5.7 \times 10^{-7}$	$5.7 \times 10^{-8}$	-	-
	750	$3.9 \times 10^{-7}$	$7.9 \times 10^{-9}$	-	-
NAFP	450	$1.1 \times 10^{-6}$	$5.0 \times 10^{-6}$	$1.7 \times 10^{-5}$	$6.8 \times 10^{-6}$
	550	$8.5 \times 10^{-5}$	$8.6 \times 10^{-6}$	$1.5 \times 10^{-4}$	$6.2 \times 10^{-6}$
	650	$6.1 \times 10^{-5}$	$1.2 \times 10^{-5}$	$8.1 \times 10^{-5}$	$2.0 \times 10^{-5}$
	750	$1.1 \times 10^{-4}$	$9.0 \times 10^{-6}$	$1.7 \times 10^{-4}$	$1.6 \times 10^{-5}$

Samples of NAFP matrices have leaching rates, on average, two orders of magnitude higher. Thus, the values of phosphorus leaching rates are about  $10^{-5}$ – $10^{-4}$  g/(cm<sup>2</sup>·day).

#### 4. Conclusions

It has been shown that obtaining FP and NAFP glass composite materials by sintering crushed pressed glass is possible at temperatures of 550–750 °C. The glass composite materials obtained at given temperatures are represented by one or more crystalline phases. FP matrices are characterized by the formation of orthophosphate phases at lower synthesis temperatures (550 °C) and pyrophosphates at higher temperatures (750 °C). NAFP matrices in this synthesis method is characterized by a more complex composition of phases with the presence of meta-, ortho-, and pyrophosphates without a clear dependence of their formation on the synthesis temperature. It has been established that glass composite material samples have a high hydrolytic stability, while FP matrix samples synthesized at 650 and 750 °C are characterized by the lowest leaching rates.

Thus, it has been shown that the proposed medium-temperature method for the synthesis of glass composite materials can be promising for the immobilization of volatile radionuclides and HLW components. Reducing the temperature of the synthesis of cured matrices by 3–5 hundreds of degrees is a significant advantage of this approach for the immobilization of HLW. This makes it possible to radically reduce the requirements for the design and operating conditions of melting equipment, significantly increase its service life, and also reduce the radioecological problems of its decommissioning. This technological approach to HLW management requires further development, including a study of the behavior and distribution of radionuclides in glass composite materials.

**Author Contributions:** Conceptualization, A.V.F. and S.S.D.; methodology, A.V.F., S.S.D. and S.E.V.; validation, A.V.F.; formal analysis, A.V.F., I.N.G. and S.S.D.; investigation, A.V.F., I.N.G. and S.S.D.; resources, S.E.V.; writing—original draft preparation, A.V.F.; writing—review and editing, S.E.V.; visualization, A.V.F. and S.E.V.; supervision, S.E.V.; project administration, S.E.V.; funding acquisition, S.E.V. All authors have read and agreed to the published version of the manuscript.

**Funding:** The work was supported by the Russian Science Foundation, project No. 22-29-01523, <https://rscf.ru/project/22-29-01523/>.

**Data Availability Statement:** Not applicable.

**Acknowledgments:** The authors thank M.A. Ivanova (Meteoritics laboratory, GEOKHI RAS) for the SEM/EDS analysis of samples.

**Conflicts of Interest:** The authors declare no conflict of interest. The funders had no role in the design of the study; in the collection, analyses, or interpretation of data; in the writing of the manuscript, or in the decision to publish the results.

#### References

1. Fedorov, Y.S.; Zil'berman, B.Y.; Aloï, A.S.; Puzikov, E.A.; Shadrin, A.Y.; Alyapyshev, M.Y. Problems of Modernization of Spent Nuclear Fuel Extraction Processing. *Russ. J. Gen. Chem.* **2011**, *81*, 1932–1948. [[CrossRef](#)]
2. Alyapyshev, M.Y.; Babain, V.A.; Ustynyuk, Y.A. Recovery of Minor Actinides from High-Level Wastes: Modern Trends. *Russ. Chem. Rev.* **2016**, *85*, 943–961. [[CrossRef](#)]
3. Lee, H. Oxide Electroreduction and Other Processes for Pyrochemical Processing of Spent Nuclear Fuels. In *Reprocessing and Recycling of Spent Nuclear Fuel*; Elsevier: Amsterdam, The Netherlands, 2015; pp. 415–436.
4. Ma, B.; Charlet, L.; Fernandez-Martinez, A.; Kang, M.; Madé, B. A Review of the Retention Mechanisms of Redox-Sensitive Radionuclides in Multi-Barrier Systems. *Appl. Geochem.* **2019**, *100*, 414–431. [[CrossRef](#)]
5. Vuori, S. The Environmental and Ethical Basis of the Geological Disposal of Long-Lived Radioactive Waste. *ATS Ydintekniikka* **1995**, *24*, 16–17.
6. Watson, L.C.; Aikin, A.M.; Bancroft, A.I. The Permanent Disposal of Highly Radioactive Wastes by Incorporation into Glass. In *Disposal of Radioactive Wastes. Vol. I. Proceedings of the Scientific Conference on the Disposal of Radioactive Wastes*; International Atomic Energy Agency (IAEA): Vienna, Austria, 1960.
7. Gregg, D.J.; Farzana, R.; Dayal, P.; Holmes, R.; Triani, G. Synroc Technology: Perspectives and Current Status (Review). *J. Am. Ceram. Soc.* **2020**, *103*, 5424–5441. [[CrossRef](#)]
8. Vance, E.R.; Chavara, D.T.; Gregg, D.J. Synroc Development—Past and Present Applications. *MRS Energy Sustain.* **2017**, *4*, 8. [[CrossRef](#)]
9. Deokattey, S.; Bhaskar, N.; Kalyane, V.L.; Kumar, V.; Jahagirdar, P.B. Borosilicate Glass and Synroc R&D for Radioactive Waste Immobilization: An International Perspective. *JOM* **2003**, *55*, 48–51. [[CrossRef](#)]

10. Ringwood, E.; Kelly, P.M. Immobilization of High-Level Waste in Ceramic Waste Forms. *Philos. Trans. R. Soc. Lond. Ser. A Math. Phys. Sci.* **1986**, *319*, 63–82. [[CrossRef](#)]
11. Ewing, R.C. Ceramic Matrices for Plutonium Disposition. *Prog. Nucl. Energy* **2007**, *49*, 635–643. [[CrossRef](#)]
12. Arinicheva, Y.; Bukaemskiy, A.; Neumeier, S.; Modolo, G.; Bosbach, D. Studies on Thermal and Mechanical Properties of Monazite-Type Ceramics for the Conditioning of Minor Actinides. *Prog. Nucl. Energy* **2014**, *72*, 144–148. [[CrossRef](#)]
13. Zhang, Y.; Vance, E.R. Plutonium in Monazite and Brabantite: Diffuse Reflectance Spectroscopy Study. *J. Nucl. Mater.* **2008**, *375*, 311–314. [[CrossRef](#)]
14. Crum, J.; Maio, V.; McCloy, J.; Scott, C.; Riley, B.; Benefiel, B.; Vienna, J.; Archibald, K.; Rodriguez, C.; Rutledge, V.; et al. Cold Crucible Induction Melter Studies for Making Glass Ceramic Waste Forms: A Feasibility Assessment. *J. Nucl. Mater.* **2014**, *444*, 481–492. [[CrossRef](#)]
15. McCloy, J.S.; Schuller, S. Vitrification of Wastes: From Unwanted to Controlled Crystallization, a Review. *Comptes Rendus Géoscience* **2022**, *354*, 1–40. [[CrossRef](#)]
16. Li, H.; Wu, L.; Wang, X.; Xu, D.; Teng, Y.; Li, Y. Crystallization Behavior and Microstructure of Barium Borosilicate Glass–Ceramics. *Ceram. Int.* **2015**, *41*, 15202–15207. [[CrossRef](#)]
17. Richerson, D.W.; Lee, W.E. *Modern Ceramic Engineering*; CRC Press: Boca Raton, FL, USA, 2018; ISBN 9780429488245.
18. Choi, J.; Um, W.; Choung, S. Development of Iron Phosphate Ceramic Waste Form to Immobilize Radioactive Waste Solution. *J. Nucl. Mater.* **2014**, *452*, 16–23. [[CrossRef](#)]
19. Poluektov, P.P.; Schmidt, O.V.; Kascheev, V.A.; Ojovan, M.I. Modelling Aqueous Corrosion of Nuclear Waste Phosphate Glass. *J. Nucl. Mater.* **2017**, *484*, 357–366. [[CrossRef](#)]
20. Lee, W.E.; Ojovan, M.I.; Stennett, M.C.; Hyatt, N.C. Immobilisation of Radioactive Waste in Glasses, Glass Composite Materials and Ceramics. *Adv. Appl. Ceram.* **2006**, *105*, 3–12. [[CrossRef](#)]
21. Soderquist, C.Z.; Schweiger, M.J.; Kim, D.-S.; Lukens, W.W.; McCloy, J.S. Redox-Dependent Solubility of Technetium in Low Activity Waste Glass. *J. Nucl. Mater.* **2014**, *449*, 173–180. [[CrossRef](#)]
22. Donald, I.W.; Metcalfe, B.L.; Fong, S.K.; Gerrard, L.A.; Strachan, D.M.; Scheele, R.D. A Glass-Encapsulated Calcium Phosphate Wasteform for the Immobilization of Actinide-, Fluoride-, and Chloride-Containing Radioactive Wastes from the Pyrochemical Reprocessing of Plutonium Metal. *J. Nucl. Mater.* **2007**, *361*, 78–93. [[CrossRef](#)]
23. Shadrin, A.Y.; Dvoeglazov, K.N.; Maslennikov, A.G.; Kashcheev, V.A.; Tretyakova, S.G.; Shmidt, O.V.; Vidanov, V.L.; Ustinov, O.A.; Volk, V.I.; Veselov, S.N.; et al. PH Process as a Technology for Reprocessing Mixed Uranium–Plutonium Fuel from BREST-OD-300 Reactor. *Radiochemistry* **2016**, *58*, 271–279. [[CrossRef](#)]
24. Simpson, M.F.; Sachdev, P. Development of Electrefiner Waste Salt Disposal Process for The Ebr- Ii Spent Fuel Treatment Project. *Nucl. Eng. Technol.* **2008**, *40*, 175–182. [[CrossRef](#)]
25. Pereira, C.; Hash, M.; Lewis, M.; Richmann, M. Ceramic-Composite Waste Forms from the Electrometallurgical Treatment of Spent Nuclear Fuel. *JOM* **1997**, *49*, 34–40. [[CrossRef](#)]
26. Priebe, S.; Bateman, K. The Ceramic Waste Form Process at Idaho National Laboratory. *Nucl. Technol.* **2008**, *162*, 199–207. [[CrossRef](#)]
27. Jena, H.; Maji, B.K.; Asuvathraman, R.; Govindan Kutty, K.V. Synthesis and Thermal Characterization of Glass Bonded Ca-Chloroapatite Matrices for Pyrochemical Chloride Waste Immobilization. *J. Non-Cryst. Solids* **2012**, *358*, 1681–1686. [[CrossRef](#)]
28. Ojovan, M.I.; Petrov, V.A.; Yudinsev, S.V. Glass Crystalline Materials as Advanced Nuclear Wasteforms. *Sustainability* **2021**, *13*, 4117. [[CrossRef](#)]
29. Stoch, P.; Ciecinska, M. Thermochemistry of Phosphate Glasses for Immobilization of Dangerous Waste. *J. Therm. Anal. Calorim.* **2012**, *108*, 705–709. [[CrossRef](#)]
30. Michie, E.M.; Grimes, R.W.; Boccaccini, A.R. Hot-Pressed Phosphate Glass–Ceramic Matrix Composites Containing Calcium Phosphate Particles for Nuclear Waste Encapsulation. *J. Mater. Sci.* **2008**, *43*, 4152–4156. [[CrossRef](#)]
31. Danilov, S.S.; Frolova, A.V.; Kulikova, S.A.; Vinokurov, S.E.; Maslakov, K.I.; Teterin, A.Y.; Teterin, Y.A.; Myasoedov, B.F. Immobilization of Rhenium as a Technetium Surrogate in Aluminum Iron Phosphate Glass. *Radiochemistry* **2021**, *63*, 99–106. [[CrossRef](#)]
32. Kulikova, S.A.; Belova, K.Y.; Tyupina, E.A.; Vinokurov, S.E. Conditioning of Spent Electrolyte Surrogate LiCl-KCl-CsCl Using Magnesium Potassium Phosphate Compound. *Energies* **2020**, *13*, 1963. [[CrossRef](#)]
33. Kulikova, S.A.; Danilov, S.S.; Matveenko, A.V.; Frolova, A.V.; Belova, K.Y.; Petrov, V.G.; Vinokurov, S.E.; Myasoedov, B.F. Perspective Compounds for Immobilization of Spent Electrolyte from Pyrochemical Processing of Spent Nuclear Fuel. *Appl. Sci.* **2021**, *11*, 11180. [[CrossRef](#)]
34. Day, D.E.; Marasinghe, K.; Ray, C.S. An Alternative Host Matrix Based on Iron Phosphate Glasses for the Vitrification of Specialized Nuclear Waste Forms; Annual Progress Report, September 15, 1996–September 14, 1997. 1997. Available online: [https://inis.iaea.org/search/search.aspx?orig\\_q=RN:31003327](https://inis.iaea.org/search/search.aspx?orig_q=RN:31003327) (accessed on 8 October 2022).
35. Brow, R.K. Review: The Structure of Simple Phosphate Glasses. *J. Non-Cryst. Solids* **2000**, *263–264*, 1–28. [[CrossRef](#)]
36. Ray, C.S.; Fang, X.; Karabulut, M.; Marasinghe, G.K.; Day, D.E. Effect of Melting Temperature and Time on Iron Valence and Crystallization of Iron Phosphate Glasses. *J. Non-Cryst. Solids* **1999**, *249*, 1–16. [[CrossRef](#)]

37. Kalmykov, S.N.; Presniakov, I.A.; Stefanovskaya, O.I.; Stefanovsky, S.V.; Myasoedov, B.F.; Glazkova, Y.S.; Sobolev, A.V.; Vinokurov, S.E. Oxidation state and coordination of iron in sodium–aluminum–iron phosphate glasses and their hydrolytic stability. *Dokl. Phys. Chem.* **2015**, *463*, 145–149. [[CrossRef](#)]
38. Danilov, S.S.; Stefanovsky, S.V.; Stefanovskaya, O.I.; Vinokurov, S.E.; Myasoedov, B.F.; Teterin, Y.A. Aluminum (iron) phosphate glasses containing rare earth and transuranium elements: Phase composition, oxidation state of Np and Pu, and hydrolytic durability. *Radiochemistry* **2018**, *60*, 434–439. [[CrossRef](#)]
39. Day, D.E.; Wu, Z.; Ray, C.S.; Hrma, P. Chemically Durable Iron Phosphate Glass Wasteforms. *J. Non-Cryst. Solids* **1998**, *241*, 1–12. [[CrossRef](#)]
40. Ren, M.; Cai, S.; Xu, G.; Ye, X.; Dou, Y.; Huang, K.; Wang, X. Influence of Heat Treatment on Crystallization and Corrosion Behavior of Calcium Phosphate Glass Coated AZ31 Magnesium Alloy by Sol–Gel Method. *J. Non-Cryst. Solids* **2013**, *369*, 69–75. [[CrossRef](#)]
41. C 1285-14; Standard Test Methods for Determining Chemical Durability of Nuclear, Hazardous, and Mixed Waste Glasses and Multiphase Glass Ceramics: The Product Consistency Test (PCT). ASTM International: West Conshohocken, PA, USA, 2014.